Laser-Wakefield Acceleration of Monoenergetic Electron Beams in the First Plasma-Wave Period

S. P. D. Mangles,[1] A. G. R. Thomas,[1] M. C. Kaluza,[1] O. Lundh,[2] F. Lindau,[2] A. Persson,[2] F. S. Tsung,[3] Z. Najmudin,[1] W. B. Mori,[3] C.-G. Wahlström,[2] and K. Krushelnick[1]

[1]*Blackett Laboratory, Imperial College London, London SW7 2BZ, United Kingdom*
[2]*Department of Physics, Lund Institute of Technology, P.O. Box 118, S-22100 Lund, Sweden*
[3]*Department of Physics and Astronomy, UCLA, Los Angeles, California 90095, USA*

(Received 8 March 2006; published 30 May 2006)

Beam profile measurements of laser-wakefield accelerated electron bunches reveal that in the monoenergetic regime the electrons are injected and accelerated at the back of the first period of the plasma wave. With pulse durations $c\tau \geq \lambda_p$, we observe an elliptical beam profile with the axis of the ellipse parallel to the axis of the laser polarization. This increase in divergence in the laser polarization direction indicates that the electrons are accelerated within the laser pulse. Reducing the plasma density (decreasing $c\tau/\lambda_p$) leads to a beam profile with less ellipticity, implying that the self-injection occurs at the rear of the first period of the plasma wave. This also demonstrates that the electron bunches are less than a plasma wavelength long, i.e., have a duration <25 fs. This interpretation is supported by 3D particle-in-cell simulations.

DOI: 10.1103/PhysRevLett.96.215001 PACS numbers: 52.38.Kd, 52.59.−f

Laser-wakefield acceleration (LWFA) has been brought closer to practical reality with recent experimental results [1–3] which demonstrated the production of narrow energy spread $\Delta E/E \simeq 3\%$ electron beams from compact, high gradient laser-plasma accelerators. LWFA works through the interaction of a short ultraintense laser pulse with a low density plasma. The ponderomotive force of the laser pulse pushes electrons away from regions of high intensity. Space charge forces due to the stationary ion background lead to the formation of a plasma wave in the wake of the laser pulse. The plasma-wave phase velocity matches the group velocity of the laser in the plasma, which, in low density plasmas, is close to (but slightly less than) the speed of light in vacuum. Because the plasma wave consists of regions of high and low electron density there is an associated longitudinal electric field with a phase velocity close to c—ideal for the acceleration of electrons. The acceleration gradients are typically orders of magnitude higher than those possible in conventional accelerators, allowing electrons with hundreds of MeV to be produced over distances on the order of a few millimeters. Such compact accelerators offer the opportunity of university scale (as opposed to national laboratory scale) radiation sources including electrons, x rays [4], and THz radiation [5].

By driving the plasma wave to large amplitude, which is generally achieved through self-focusing and pulse compression of the driving laser pulse in the wake itself in a positive feedback process, it is possible to inject background electrons into the plasma wave to be accelerated, removing the need for external injection mechanisms. Prior to the experimental results reported in [1–3] and the simulations presented in [6], the electron energy distribution measured in self-injected wakefield acceleration experiments were always "quasi-Maxwellian," having an exponential reduction in number towards high energies.

With a sufficiently short high-intensity pulse, or with sufficient self-modulation and compression, it is possible to enter the "bubble" regime [6,7] (similar to the "blow-out" regime in particle driven wakefield accelerators [8]). Here a short pulse is defined to be one where the pulse length is comparable to the wavelength of the plasma wave it generates, i.e., when $c\tau \simeq \lambda_p$ [τ is the FWHM duration of the laser pulse and λ_p is the wavelength of a relativistic plasma wave; $\lambda_p = 2\pi c/\omega_p$; ω_p is the plasma frequency $\omega_p = (n_e e^2/m_e \epsilon_0)^{1/2}$]. In the bubble regime the electrons are pushed away so strongly by the laser pulse that a plasma cavity (i.e., a region devoid of electrons) forms behind the laser. Because the heavy plasma ions are much less affected by the ponderomotive force the cavity has a strong electric field which has ideal accelerating properties including linear accelerating and focusing fields.

Simulations of recent experiments which produced monoenergetic electron beams have shown that the electrons are trapped within the first period of the plasma wave. This has been difficult to test experimentally because the physical size and duration of the injected bunch are small and the electron bunch is within the plasma bubble, making probing (with, for example, laser or particle sources) difficult.

In this Letter, we report a measurement that demonstrates that the high-energy electrons are indeed injected into the rear of the first plasma-wave period. Measurements of the transverse profile of the electron beam in a LWFA experiment reveal that, when the laser pulse length is comparable to the plasma wavelength, the electron beam profile is elliptical. This is due to an increase in the beam emittance in the plane of polarization of the laser caused by

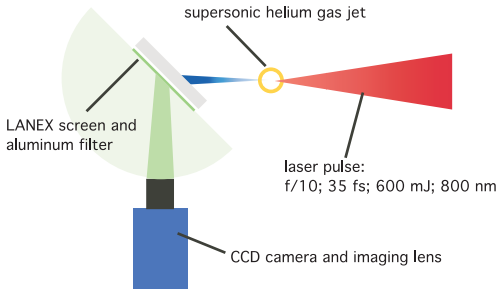

FIG. 1 (color online). Schematic of the experimental setup shown from above.

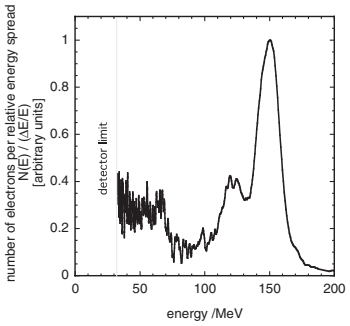

FIG. 2. Example electron spectrum taken at a plasma density of $n_e = 2 \times 10^{19}$ cm^{-3} with laser parameters of $\tau = 35$ fs, $E = 600$ mJ.

the interaction of the electrons with the laser electric field. When the pulse length is made shorter than the plasma wavelength the degree of ellipticity decreases, confirming that this effect is indeed due the interaction with the laser pulse.

The experiments were performed with the 10 Hz multi-THz femtosecond laser at the Lund Laser Centre, a Ti:sapphire system delivering 35 fs pulses of up to 35 TW at a central wavelength of 800 nm. The laser pulses are focused onto the edge of a supersonic gas jet using an $f/10$ off-axis parabolic mirror. The experimental setup is shown in Fig. 1. The gas jet is capable of producing electron densities in the range $(0.5\text{–}5) \times 10^{10}$ cm^{-3}. Measurements of the electron energy distribution were performed using a magnetic spectrometer with a scintillating screen (Kodak Lanex) and CCD imaging system as the detector. These show the production of narrow energy spread electron beams over a range of densities with energies up to 200 MeV and energy spreads of a few percent. An example electron spectrum is shown in Fig. 2 taken at a plasma density of $n_e = 2 \times 10^{19}$ cm^{-3}.

A separate Lanex screen could be inserted into the path of the electron beam to allow the electron beam profile to be measured. The screen was 320 ± 10 mm from the laser focus. A 12 mm layer of aluminum is placed in front of this screen so that the beam profile was due to electrons with energies above ≈ 7 MeV. Scattering through the aluminum plate for the high-energy electron beam contributes to less than 5% of the beam size for electron energies greater than 70 MeV (corresponding to the majority of the electron signal above 7 MeV). The scintillator screen emits light through 2π sr and can therefore be viewed from a range of angles. By placing the screen at 45° to the beam propagation direction and imaging the screen from a viewing angle of 90° we could observe the electron beam profile without any projection error and without the need to place mirrors or detectors into the electron beam path behind the screen.

A zero order mica $\lambda/2$ plate was placed in the unfocused laser beam to allow the plane of polarization to be continuously rotated, allowing any effects of the laser polarization on the beam profile to be investigated. The plasma density in the gas jet was obtained from forward Raman scattering measurements. These were performed by detuning the grating compressor resulting in a significantly longer laser pulse ($c\tau \gg \lambda_p$) than that used in the electron acceleration experiments as the growth rate of forward Raman scattering is too small in the regime where $c\tau \simeq \lambda_p$ [9].

The first set of results presented were obtained with a pulse duration of 68 fs and a plasma density of 2.2×10^{19} cm^{-3}, i.e., with $c\tau \simeq 3\lambda_p$. The beam profile of the electron beam ($E > 7$ MeV) was measured as described above for various polarization angles. Figure 3 shows some typical beam profiles. The profiles are clearly elliptical and the axis of the ellipse is directly correlated with the polarization of the laser.

To quantify the electron beam ellipticity an ellipse is fitted to the half-maximum contour of the profile, hence the eccentricity of the ellipse $\epsilon = \sqrt{(1 - b^2/a^2)}$, where a and b are the major and minor axes of the ellipse, can be calculated for each profile. Figure 4 shows how the tilt angle of the ellipse varied with the laser polarization. A direct correlation is revealed by a least-square fit to the data, indicating a gradient close to unity of 1.09 ± 0.06 and a correlation coefficient of $R^2 = 0.77$. The error bars represent our estimate of a systematic error in the laser polarization angle after insertion of the wave plate. The fluctuations in the beam profile tilt are probably due to shot-to-shot fluctuations in the experimental parameters, the main sources of fluctuation include the laser energy, pulse duration, focal spot, and plasma profile. The fact that the

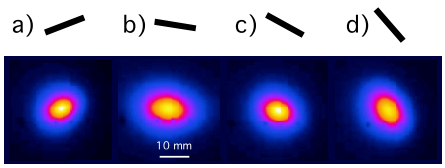

FIG. 3 (color online). Representative data showing the variation of electron beam profile with laser polarization at $n_e = 2.2 \times 10^{19}$ cm^{-3} with a pulse duration of 68 fs. The black line indicates the laser polarization angle ±5°. (a) −20°, (b) 10°, (c) 30°, and (d) 50°.

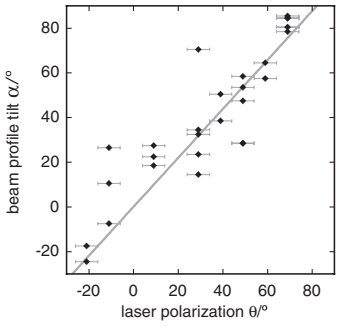

FIG. 4. Variation of electron beam profile tilt with respect to laser polarization. Black squares: experimental data. Gray line: least-squares linear fit, gradient 1.09 ± 0.07.

elliptical profile varies with the laser polarization indicates that it is not caused by an asymmetry in the focal spot. The effect on the focal spot after insertion of the wave plate has been tested and shown to be negligible. Measurements of the electron beam profile farther downstream show a larger eccentricity indicating that the ellipticity is a signature of an asymmetry in the transverse emittance rather than simply an asymmetric beam divergence.

With a shorter laser pulse duration of 35 fs we were able to observe the variation of the electron beam profile shape over a range of plasma densities. This part of the experiment was performed with the $\lambda/2$ plate removed from the setup.

Figure 5 shows four typical electron beam profiles at various plasma densities. The beam is highly collimated with a divergence angle of less than 25 mrad over the range of densities studied. The analyzed data from a number of beam profiles is shown in Fig. 6. At the lowest density the electron beam has the lowest ellipticity ($\epsilon = 0.63 \pm 0.08$ at $n_e = 2.1 \times 10^{19}$ cm^{-3}) and the beam becomes more elliptical as the plasma density is increased. The peak ellipticity observed was at $n_e = 2.7 \times 10^{19}$ cm^{-3} with $\epsilon = 0.77 \pm 0.03$. When the density was increased further the beam divergence at 90° to the laser polarization increased, leading to a more divergent but more circular beam.

The fact that the electron beam ellipticity reduces as the ratio $c\tau/\lambda_p$ reduces implies that the electrons spatially overlap the laser pulse and in fact stem from the back of the first wave period. Extrapolation of the eccentricity data

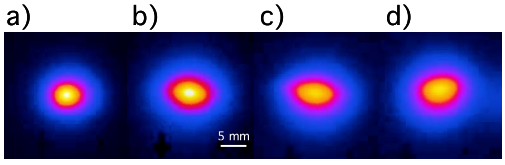

FIG. 5 (color online). Four typical electron beam profile measurements at various plasma densities. (a) $n_e = 2.1 \times 10^{19}$ cm^{-3}, (b) $n_e = 2.4 \times 10^{19}$ cm^{-3}, (c) 2.7×10^{19} cm^{-3}, and (d) 3.0×10^{19} cm^{-3}. The laser polarization is horizontal.

(from the lowest three densities measured) to still lower densities reveals that the beam profile is expected to be circular (i.e., $\epsilon = 0$) at a plasma density corresponding to $c\tau \approx \lambda_p/2$ as shown in the inset of Fig. 6(a). Extrapolation of the beam size data is also not inconsistent with a circular beam close to $c\tau = \lambda_p/2$. This is because the bubble is approximately λ_p long and the electrons only extend into the bubble by half a plasma wavelength, as this is the dephasing point. This implies that the electron bunches in this experiments are less than a plasma wavelength long and therefore have a duration of less than 25 fs at a plasma density of $n_e = 2.1 \times 10^{19}$ cm^{-3}.

At lower density, λ_p is longer and the laser pulse occupies a smaller fraction at the front of the plasma wave. In the regime where $c\tau < 2\lambda_p$ the intensity of laser light at the back of the first wave period is reduced for longer plasma wavelengths, i.e., lower electron densities. Hence, if the electrons are generated at the back of the first wave period, then at low densities the effect of the laser field on the electron motion will be reduced, as observed experimentally. The observed increase in the divergence at 90° to the laser polarization at high density is probably because the effects of the transverse plasma fields are greater than the effect of the interaction with the laser field. This is due to the increase in the plasma-wave electric field and the decrease of the transverse size of the plasma wave with increasing density. This is probably why these effects have not been observed in earlier self-modulated wakefield experiments.

Earlier theoretical work on multidimensional wave breaking suggested that transverse wave breaking occurs more easily farther behind the laser pulse [10] due to an increase in the curvature of the wakefield, and hence we might have expected the electron injection to occur in trailing wave periods. The fact that the electrons in our

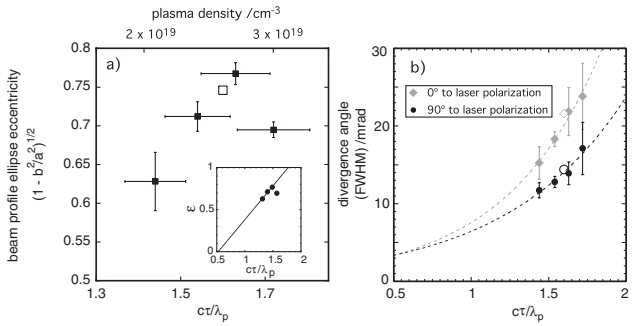

FIG. 6. (a) Variation of electron beam profile ellipticity with plasma density (top axis) and ratio of pulse duration to plasma wavelength, $c\tau/\lambda_p$ (bottom axis). Inset shows the same data with an extrapolation to $\epsilon = 0$. (b) Variation of the electron beam divergence with the ratio $c\tau/\lambda_p$. Diamonds: beam divergence in the plane of polarization of the laser. Circles: beam divergence 90° to the plane of laser polarization. Open symbols are data from the 3D particle-in-cell simulation described in the text.

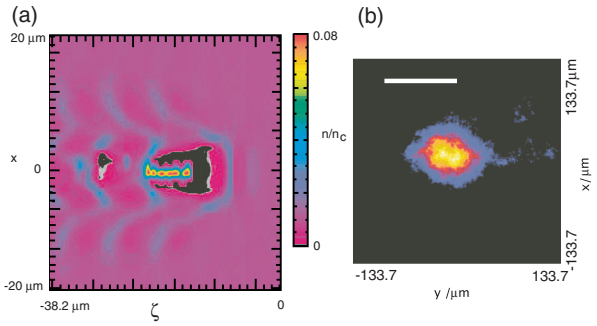

FIG. 7 (color online). (a) Electron density in x-ξ plane from a 3D simulation (described in the text) showing injection of electrons at the rear of the first plasma-wave period. (b) Projection of the electron beam profile 2.3 mm from focus; the white line indicates the laser polarization.

experiments come from the first wave period is strong evidence that the wakefield structure is more like the bubble regime first described in [6], although it is likely that some evolution of the laser pulse (i.e., self-focusing and pulse compression in the wakefield) must occur before the bubble regime is reached. Simulations of similar experimental parameters have already been reported [1–3,11–14].

Results from a 3D simulation performed at a density where $c\tau = 1.6\lambda_p$ are presented in Fig. 7. The pulse parameters correspond to a peak vacuum intensity of 5×10^{18} W cm^{-2} in a focal waist of $w_0 = 12.5$ μm. The pulse duration (FWHM) $\tau = 40$ fs and $n_e = 2 \times 10^{19}$ cm^{-3}. The simulation window moves along the laser propagation direction at the speed of light ($\xi = z - ct$ is the direction of laser propagation, and x and y are the transverse coordinates). The resolution of the simulation was carefully chosen to minimize numerical dispersion effects, with 40 cells/λ_0 in the laser propagation direction and 27 cells/λ_p in the transverse dimensions. This resolution was chosen as the result of a series of 2D simulations as discussed in [15].

Figure 7(a) shows a cross section (at $y = 0$) of the electron density in the simulation. The high density "stem" of electrons emanating from the back of the bubble are the self-injected electrons. At this density the electrons interact with the laser field, resulting in a larger transverse emittance in the plane of laser polarization. It is this motion in the laser field which gives rise to the elliptical beam profile shape observed in the experiment. The projected x-y profile of the electron beam ($E > 10$ MeV) from the 3D simulation is shown in Fig. 7(b). This profile is calculated from the trajectories of electrons at the end of the simulation and is projected 0.3 mm from the end of the plasma (2.3 mm from the laser focus). There is a clear ellipticity to the beam profile, with the divergence angle for electrons with $E > 10$ MeV (FWHM) being 22 mrad in the plane of laser polarization and 14 mrad at 90° to the laser polarization. The eccentricity of this profile, calculated using the same method as the experimental profiles, is $\epsilon = 0.75$. The electron beam eccentricity and divergence from the simulation are shown as open symbols in Fig. 6 and are in good agreement with the experimentally observed values.

The agreement between 3D particle-in-cell simulations and laser-plasma acceleration experiments can be excellent in terms of the principal output (e.g., the electron spectra in [3]). However, it is more difficult to ensure that the physical processes, such as electron injection, are accurately described by the numerical modeling. The results described here help to improve our confidence in the numerical modeling techniques employed.

These results also show experimentally that the best quality electron bunches, especially in terms of transverse emittance, will be produced when the ratio of pulse duration to plasma wavelength is small, as was discussed in [16]. It may also be possible to reduce the emittance even in the case of $c\tau \simeq \lambda_p$ with the use of circularly polarized laser pulses; however, this is a subject for further investigation.

We acknowledge support from the Swedish Research Council, the Knut and Alice Wallenberg foundation, the EU Access to Research Infrastructures Programme (RII3-CT-2003-506350 Laserlab Europe) and Research Councils U.K.

[1] S. P. D. Mangles *et al.*, Nature (London) **431**, 535 (2004).
[2] C. G. R. Geddes *et al.*, Nature (London) **431**, 538 (2004).
[3] J. Faure *et al.*, Nature (London) **431**, 541 (2004).
[4] A. Rousse *et al.*, Phys. Rev. Lett. **93**, 135005 (2004).
[5] W. P. Leemans *et al.*, Phys. Rev. Lett. **91**, 074802 (2003).
[6] A. Pukhov and J. Meyer-ter Vehn, Appl. Phys. B **74**, 355 (2002).
[7] I. Kostyukov, A. Pukhov, and S. Kiselev, Phys. Plasmas **11**, 5256 (2004).
[8] J. B. Rosenzweig *et al.*, Phys. Rev. A **44**, R6189 (1991).
[9] W. B. Mori, IEEE J. Quantum Electron. **33**, 1942 (1997).
[10] S. V. Bulanov *et al.*, Phys. Rev. Lett. **78**, 4205 (1997).
[11] F. S. Tsung *et al.*, Phys. Rev. Lett. **93**, 185002 (2004).
[12] K. Krushelnick *et al.*, Phys. Plasmas **12**, 056711 (2005).
[13] C. G. R. Geddes *et al.*, Phys. Plasmas **12**, 056709 (2005).
[14] V. Malka *et al.*, Phys. Plasmas **12**, 056702 (2005).
[15] F. S. Tsung *et al.*, Phys. Plasmas (to be published).
[16] V. Malka *et al.*, Science **298**, 1596 (2002).